Article ID: 1000-9116(2003)02-0205-08

Rupture directivity and hanging wall effect in near field strong ground motion simulation*

TAO Xia-xin[1, 2) (陶夏新) WANG Guo-xin[3) (王国新)

1) *Harbin Institute of Technology, Harbin* 150001, *China*
2) *Institute of Engineering Mechanics, China seismological bureau, Harbin* 150080, *China*
3) *Dalian Institute of Technology, Dalian* 116024, *China*

Abstract

A random synthesis procedure based on finite fault model is adopted for near field strong ground motion simulation in this paper. The fault plane of the source is divided into a number of sub-sources, the whole moment magnitude is also divided into more sub-events. The Fourier spectrum of ground motion caused by a sub-event in given sub-source, then can be derived by means of taking the point source spectrum, attenuation with distance, energy dissipation, and near surface effect, into account. A time history is synthesized from this amplitude spectrum and a random phase spectrum, and being combined with an envelope function. The ground motion is worked out by superposition of all time histories from each sub-event in each sub-source, with time lags determining by the differences between the triggering times of sub-events and distances of the sub-sources. From the example of simulations at 21 near field points in a scenario earthquake with 4 dip angles of the fault plane, it is illustrated that the procedure can describe the rupture directivity and hanging wall effect very well. To validate the procedure, the response spectra and time histories recorded at three near fault stations MCN, LV3 and PCD during the Northridge earthquake in 1994, are compared with the simulated ones.

Key words: **near field strong ground motion; rupture directivity; hanging wall; source; random synthesis**
CLC number: P315.3 **Document code**: A

Introduction

Strong ground motion simulation provides input for earthquake response analysis of critical facilities. The key point in the simulation is to characterize all of the engineering features of the motion. In general, it is believed that the widely adopted empirical attenuation relationships cannot describe some engineering features of ground motion in near field.

In the past ten odd years, strong ground motion records were accumulated very much faster than before, especially during the Loma Prieta (1989, M=7.1), Northridge (1994, M=6.7), Kobe (1995, M=6.9) and Jiji (1999, M=7.3) earthquakes, there were tens or more than hundred

*Received date: 2002-04-15; revised date: 2002-09-02; accepted date: 2002-10-08
Foundation item: Earthquake Science Foundation under Contract No.201009

accelerograms recorded in each event. Some significant engineering characteristics, such as near-fault rupture directivity effect, hanging wall effect, crustal wave guide effect and basin edge effect, were recognized from the recordings (Somerville, 2000). The former two strongly influence the distribution of ground motion amplitudes on rock sites in the near fault region. Since the currently adopted empirical attenuation relationships cannot take these effects into account, some researchers improved form of relation with additional complexity to obtain a little flexibility (Somerville, *et al*, 1997; Abrahamson, Silva, 1997).

In this paper, a random synthesis procedure based on finite fault model, naturally a numerical model, is adopted for simulating the near filed strong ground motion. The near-fault rupture directivity and hanging wall effect can be found obviously from the results. It can be recommended in practical seismic hazard assessment for rock site in near field.

As well known, ground motion depends on the earthquake source, the wave propagation path from the source to the site, and the local site condition. The latter is very complicated, usually needs specific study. In this paper, just the former two are taken into account for rock sites. Of course, the result can be the input of the analysis of the latter.

1 The rupture directivity effect and the hanging wall effect

The distribution of ground motion amplitudes in near-fault area is strongly influenced by the fault geometry. The rupture directivity effect in ground motion at a site is caused by the rupture propagation and the radiation pattern of the shear dislocation on the fault. Forward rupture directivity effect occurs when the rupture front propagates toward the site, and the direction of slip on the fault is aligned with the site. The ground motion at the site will be with shorter duration, and larger response spectrum amplitude. Backward directivity effect, which occurs when the rupture propagates away from the site, induces long duration motion having low amplitudes at long periods.

If the waves from the sub-ruptures on the faulting plane arrive at the site in a time period short enough, there will be a quite large acceleration pulse in the ground motion with long period. The periods of the pulses recorded in some earthquakes lie in the range of 1 to 2 seconds, comparable to the natural periods of structures such as bridges and mid-rise buildings. Many of those structures may be severely damaged under the action of the pulses (Somerville, 2000).

Near fault rupture directivity effect can be significant at periods longer than 1 second and at distances less than about 50 km, with the intensity of the effect depending on the earthquake magnitude and on the geometry relation between the site and the fault. The forward directivity effects are expected to be most concentrated away from the hypocenter for strike-slip faulting, and dip slip faulting produces directivity effects on the ground surface that are most concentrated up dip from the hypocenter. The effect of forward rupture directivity on the response spectrum is to increase the level of the response spectrum of the horizontal component normal to the fault strike at periods longer than 0.5 seconds. This causes the peak response spectral acceleration of the strike-normal component to shift to longer periods.

The hanging wall effect is due mainly to the proximity of the fault plane to hanging wall sites. It is most pronounced for periods shorter than about 1 second, and occurs away from the top edge of the fault on the hanging wall side. Sites on the hanging wall of a dipping fault have closer proximity to the fault as a whole than do sites at the same closest distance on the footwall. This causes larger short period ground motions on the hanging wall than on the footwall at the same

total number of sub-events in the k^{th}–m^{th} sub-source, and a_{km} is the time history generated by the k^{th}–m^{th} sub-source, t_{kmn} represents the time lag from the difference between the triggering of the sub-events, and the difference between the paths from the sub-sources to the site.

2.2 The Fourier spectrum of ground motion at site from a point source

The acceleration Fourier spectrum radiated from a point source can be calculated by equation 3 (Hanks, McGuire, 1981; Silva, *et al*, 1990; Beresnev, Atkinson, 1997; Atkinson, Silva, 2000),

$$FA(M_0, f, R) = C \cdot S(M_0, f) \cdot G(R) \cdot D(R, f) \cdot A(f) \cdot P(f) \cdot I(f) \tag{3}$$

where $FA(M_0, f, R)$ is the Fourier amplitude spectrum of ground motion at a site with distance R, C is a scaling factor, $S(M_0, f)$ is the source spectrum, $G(R)$ accounts for the geometrical attenuation caused by the changing of wave component along the distance, $D(R, f)$ represents anelastic attenuation, $A(f)$ is near surface amplification factor and can be estimated by a transfer function of regional crust velocity gradient, $P(f)$ is a high-cut filter, $I(f)$ represents the relation between the acceleration spectrum and displacement spectrum.

An improved source spectral model (Masuda, 1982) is adopted with parameters depending on the statistical analysis of the strong motion recordings (WANG, TAO, 2001).

$$S(M_0, f) = \frac{M_0}{\left[1 + \left(\frac{f}{f_0}\right)^a\right]^b} \tag{4}$$

where M_0 is moment magnitude, f is frequency, f_0 is corner frequency. The coefficients a and b are magnitude dependent, as following

$$a=3.05-3.33M \qquad b=2.0/a \tag{5}$$

One can find that the model embodies the differences between small and strong earthquakes not only in amplitudes and corner periods, but also in the shapes that were revealed by the recordings.

3 A numerical example of strong ground motion simulation

The Northridge M=6.7 earthquake in the United States, 1994, with a maximum dislocation of 3 m, is taken as an example for strong ground motion simulation.

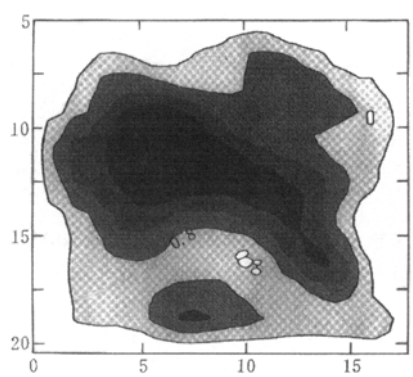

Figure 1 Dislocation distribution on the faulting plane of Northridge earthquake

The full fault dimension of Northridge earthquake was estimated as 18 km×15 km along strike and dip respectively (Wald, *et al*, 1996). The parameters of the source are listed in Table 1, and the dislocation distribution is shown in Figure 1 (Beresnev, Atkinson, 1998). The sub-event magnitude is chosen as 5.0 in this study, the fault is discretized into sub-sources, each 3 km×3 km (Wang, Tao, 2001), and the individual slips are derived based on the counters from the model of Wald, *et al*. Totally, there are 30 sub-sources on the main shock rupture plane, and the dislocation

values for each one are shown in Figure 2. According to the relation between earthquake moments of magnitude 6.7 and 5.0, the total number of sub-events is calculated as 79. Then these events are distributed into the sun-sources with weighting factors of dislocation values. The ground motions are simulated for 3 station sites where ground motions were recorded during the shock. The rupture starts at the sub-source with the dislocation value in square frame.

Table 1 Source parameters of Northridge earthquake

Fault strike/dip	Fault (L×W) /km×km	Fault depth /km	Earthquake moment $/10^{19}$ N·m	Stress drop $/10^5$ Pa	v_S /km·s^{-1}	Media density. /g·cm^{-3}	Rapture velocity /km·s^{-1}
122°/40°	18×15	5~21	1.1±0.2	50	3.7	2.8	0.8×3.7

3.1 Comparison of the ground motion simulation with the records at 3 near field sites

In order to validate the simulation procedure, the results firstly compared with the ground records at station PCD, LV3 and MCN run by USGS and CDMG, which are all rock sites with hypocenter distance 27.1, 54.5 and 27.2 km respectively. For each site, 5 accelerograms are synthesized for horizontal component. The average response spectrum of the 5 spectra with damping ratio 5% at each station expressed as solid line is compared with that of the two recorded horizontal components expressed as dashed and dotted lines respectively, in Figure 3. One accelerogram of the 5 for each station is also shown in the right side of Figure 3 with the records (the above two) together. The horizontal axes are for period in second at left side, and for time in second at right. One can find the fact that the spectra are quite consistent, while the envelops of the time histories are yet with some difference.

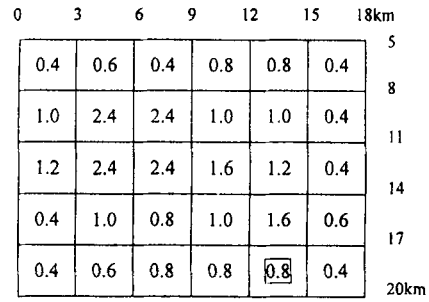

Figure 2 The numerically simplified dislocation distribution

3.2 The rupture directivity and hanging wall effect in the ground motion simulation

Assume the rupture starts from the left-down corner of the faulting plane. The rupture directivity effect can be recognized obviously from the results at the sites on the strike line, respectively marked as L0 and R0 for sites at the ends and L10 to L50 on left and R10 to R50 on right which is 10, 20, 30, 40, 50 km from the two ends, and M for that at the center. The hanging wall effect can be found from the results at the sites on the perpendicular line cross the center, respectively marked as U10 to U50 on the footwall with distance 10, 20, 30, 40, 50 km to the center, and D10 to D50 on the hanging wall. In order to examine the effect of the dip angle, the simulations are carried out with 4 angles varying from 90° to 30°. The peak acceleration (PGA) values are shown in Figure 4. One can see that PGA gets larger along the rupture forward direction, about 20% than those at the backward direction at distance 30 to 40 km, and is close to that at 50 km, while the difference is maximum for dip angle 30°. In brief, the rupture directivity effect and hanging wall effect on response spectra are shown in Figure 5 and Figure 6, for sites 10, 30, 50 km from the two ends and for sites 20 and 40 km from the center. The horizontal axes are for period in second and the vertical axes for amplitude of response spectra in CM/SEC/SEC. One can find that the heightening of response spectra by the rupture directivity effect is 20% mainly in the period range about 0.2~0.7 second, and gets maximum for dip angle 30°and 45°. While the heightening

of response spectra by the hanging wall effect is about 50% in a much wider period range less than 1 second.

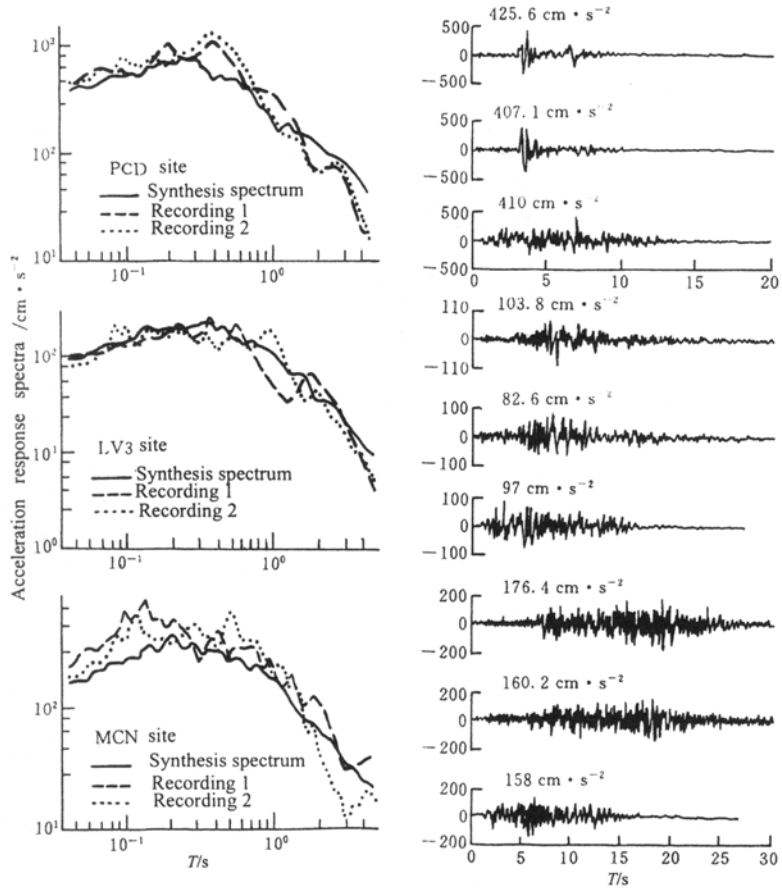

Figure 3. Comparison of the simulation with the records

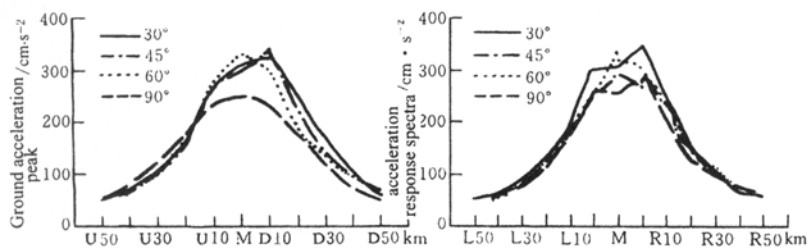

Figure 4. The rupture directivity and hanging wall effect on PGA

4 Conclusions

In the paper, the authors pointed out that the currently adopted design ground motion simulation procedure to match a design spectrum is not valid, if the design spectrum explicitly

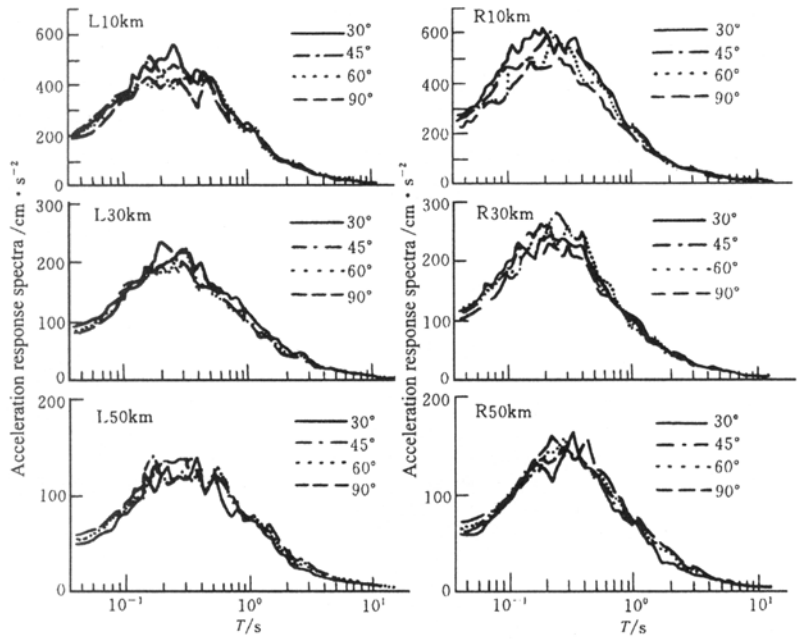

Figure 5. The rupture directivity effect on response spectra

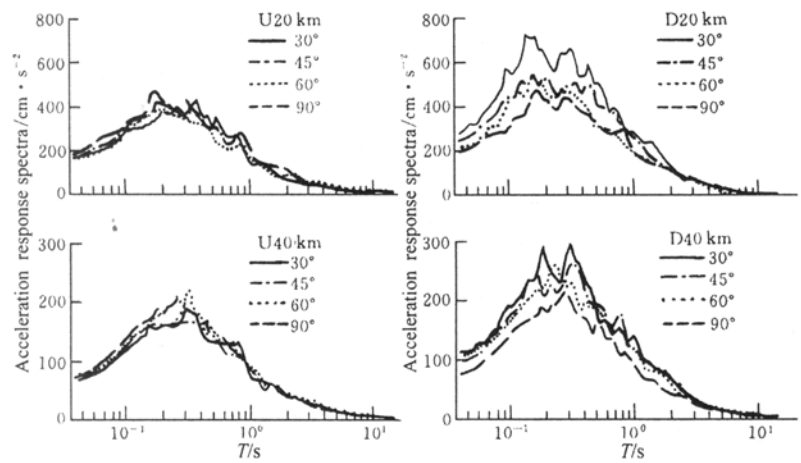

Figure 6. The hanging wall effect on response spectra

incorporates near-fault conditions. The spectral matching process cannot express the rupture directivity and hanging wall effect during the generated time histories. And it is also difficult to select appropriate records, because the effects are present in some but not recorded in all near-fault strong motion. As an improvement, a random synthesis procedure based on finite fault model is introduced. From a numerical example of the Northridge earthquake, the advantage of the procedure is validated. The heightening of PGA and response spectra amplitudes can be 20% and 50% by the directivity effect and the hanging wall effect, respectively.

It is also obvious that some other near field effect of ground motion has not yet be examined

in this paper, such as the long period near field acceleration pulse, the relativity between the two horizontal components, permanent displacements in near-fault ground displacements due to the static displacement field of the earthquake. That means the procedure needs to be improved further to take the orientation of the fault and of the static and dynamic ground displacements into account. The former can be included in *C*, the first term of the right side of equation 3.

The spatial correlation between the multi-points in a site area can be simulated by means of the introduced procedure directly. The authors will write another paper on it.

References

Abrahamson N A, Silva W J. 1997. Empirical response spectral attenuation relations for shallow crustal earthquakes [J]. *Seism Res Lett*, **68**(1): 94~127.

Atkinson G, Silva W. 2000. Stochastic modeling of California ground motions [J]. *Bull Seism Soc Amer*, **90**(2): 255~274

Atkinson G. 1984. Attenuation of strong ground motion in Canada from a random vibrations approach [J]. *Bull Seism Soc Amer*, **74**(6): 2 629~2 653.

Atkinson G,Boore D M.1997. Stochastic point-source modeling of ground motion in the Cascadia region [J]. *Seism Res Lett*, **68**(1):74~85.

Beresnev I A, Atkinson G. 1997. Modeling finite-fault radiation from the ω^n spectrum [J]. *Bull Seism Soc Amer*, **87**(1): 67~84.

Beresnev I A, Atkinson G. 1998. Stochastic finite-fault modeling of ground motions from the 1994 Northridge, California, earthquake, I. Validation on rock sites [J]. *Bull Seism Soc Amer*, **88**(6): 1 392~1 401.

Beresnev I A, Atkinson G. 1999. Genetic finite-fault model for ground-motion prediction in Eastern North America [J]. *Bull Seism Soc Amer*, **89**(3): 608~625.

Boore D, Atkinson G. 1987. Stochastic prediction of ground motion and spectral response parameters at hard-rock sites in Eastern North America [J]. *Bull Seism Soc Amer*, **77**(2): 440~467.

Boore D. 1983. Stochastic simulation of high-frequency ground motions based on seismological models of the radiated spectra [J]. *Bull Seism Soc Amer*, **73**(6): 1 865~1 894.

Hanks T C, McGuire R K. 1981. The character of high-frequency strong ground motion [J]. *Bull Seism Soc Amer*, **71**(6): 2 071~2 095.

Irikura K. 2000. Prediction of strong motions from future earthquakes caused by active faults—case of the Osaka basin [A]. In: Proceedings. of 12th World Conference on Earthquake Engineering [C]. Auckland: IAEE, 2 687.

Masuda T. 1982. Scaling relations for source parameters of microearthquakes in the Northeastern part of Japan [D]. Tohoku Univ.

Silva W, Darragh R, Stark, *et al*. 1990. A methodology to estimate design response spectra in the near source region of large earehquakes using the band-limited-white-noise ground motion model [A]. *Proceedings of National Conference on Eart Eng* [C]. Palm Spring: EERI,487~494.

Sokolov V. 1997. Empirical models for estimation Fourier-amplitude spectra of ground acceleration in the Northern Caucasus (Racha seismological zone) [J]. *Bull Seism Soc Amer*, **87**(6): 1 401~1 412.

Somerville P. 2000. Seismic hazard evaluation [A]. In: Proceedings. of 12th World Conference on Earthquake Engineering [C]. Auckland: IAEE, 2 833.

Somerville P G,Smith N F, W Graves R, *et al*. 1997. Model of strong ground motion attenuation relations to include the amplitude and duration effects of rupture directivity [J]. *Seism Res Lett*, **68**(1): 199~222.

Toro G, Abrahamson N A, Schneider J F. 1997. Model of strong ground motions from earthquakes in Central and Eastern North America: Best estimates and uncertainties [J]. *Seism Res Lett*, **68**(1): 41~57.

Toro G, McGuire R. 1987. An investigation into earthquake ground motion characteristics in Eastern North America [J]. *Bull Seism Soc Amer*, **77**(4): 468~489.

Wald D J, Heaton T H, Hudnut K W. 1996. The slip history of the 1994 Northridge, California, earthquake determined from strong-motion, teleseismic, GPS, and leveling data [J]. *Bull Seism Soc Amer*, **86**(1B): S49~S57.

WANG Guo-xin, TAO Xia-xin. 2001 Strong ground motion of the 1994 *M*6.7 Northridge earthquake simulated by a stochastic approach [A], In: Proc. of IAGA-IASPEI Joint Scientific Assembly [C], Hanoi: IASPEI.